

Improved Wind and Precipitation Forecasts over South China Using a Modified Orographic Drag Parameterization Scheme

ZHONG Shuixin^{1,2*} (钟水新) and CHEN Zitong¹ (陈子通)

¹ Institute of Tropical and Marine Meteorology/Guangdong Provincial Key Laboratory of Regional Numerical Weather Prediction, China Meteorological Administration, Guangzhou 510080

² State Key Laboratory of Severe Weather, Chinese Academy of Meteorological Sciences, Beijing 100081

(Received February 28, 2014; in final form September 2, 2014)

ABSTRACT

To improve the wind and precipitation forecasts over South China, a modified orographic drag parameterization (OP) scheme that considers both the gravity wave drag (GWD) and the mountain blocking drag (MBD) effects was implemented in the Global/Regional Assimilation and Prediction System Tropical Mesoscale Model (GRAPES_TMM). Simulations were performed over one month starting from 1200 UTC 19 June 2013. The initial and lateral boundary conditions were obtained from the NCEP global forecast system output. The simulation results were compared among a control (CTL) experiment without the OP scheme, a GWDO experiment with the OP scheme that considers only the GWD effect, and an MBD experiment with the modified OP scheme (including both GWD and MBD). The simulation with the modified OP scheme successfully captured the main features of precipitation, including its distribution and intensity, and improved the wind circulation forecast in the lower troposphere. The modified OP scheme appears to improve the wind forecast by accelerating the ascending air motion and reinforcing the convergence in the rainfall area. Overall, the modified OP scheme exerts positive impacts on the forecast of large-scale atmospheric fields in South China.

Key words: orographic drag parameterization (OP), gravity wave drag (GWD), wind circulation, South China

Citation: Zhong Shuixin and Chen Zitong, 2015: Improved wind and precipitation forecasts over South China using a modified orographic drag parameterization scheme. *J. Meteor. Res.*, **29**(1), 132–143, doi: 10.1007/s13351-014-4934-1.

1. Introduction

The dynamic and thermal effects of large-scale orography can significantly impact the atmospheric circulations and climate patterns. In large-scale atmospheric models, the gravity waves (GWs) induced by subgrid-scale orography (SSO) largely influence the wind and temperature in the middle troposphere (e.g., Palmer et al., 1986; Kim and Arakawa, 1995; McLandress et al., 2012). The dissipation of GWs generates synoptic-scale forces on the atmospheric flow, known as gravity wave drag (GWD). Simulations of short-term evolution of weather systems and long-term cli-

mate change are improved with parameterization of the GWD induced by SSO (Lilly, 1972; Matsuno, 1982; Boer et al., 1984). Without parameterization of the subgrid-scale GWD, excessively strong westerlies (easterlies) may appear in the simulations of the winter (summer) midlatitude Northern Hemisphere (Palmer and Mansfield, 1986; Kim et al., 1998; Bauer et al., 2000).

In the early atmospheric models, parameterization of the GWD induced by SSO was based on the two-dimensional linear wave theory that describes orographic GWs (e.g., Helfand et al., 1987; Miller et al., 1989; Broccoli and Manabe, 1992) with the “satura-

Supported by the Science and Technology Key Project of the South China Regional Meteorological Center (GRMC2014M05), China Meteorological Administration Special Public Welfare Research Fund (GYHY201406003 and GYHY201206010), National Natural Science Foundation of China (41075083 and 41075040), and Science and Technology Project of Guangdong Province (2011A032100006 and 2012A061400012).

*Corresponding author: sxzhong@grmc.gov.cn.

©The Chinese Meteorological Society and Springer-Verlag Berlin Heidelberg 2015

tion hypothesis” (Lindzen, 1981). Boer et al. (1984) first considered the influence of GWD on lower-level atmospheric circulations in large-scale models. The effect of wave breaking on GWD, first considered by Palmer and Mansfield (1986) in a saturation theory framework, has been adopted in many later studies (Helfand and Labraga, 1988; Miller et al., 1989; Qian, 2000). Besides improving the low-level atmospheric circulation simulations, the GWD parameterization alleviates the simulation system bias, such as the warm pool effect caused by southerly deviation, leading to improved simulations of large-scale atmospheric fields at upper levels in the Northern Hemisphere (Hong et al., 2008; McLandress et al., 2013).

The GWD parameterization scheme of Kim and Arakawa (1995; hereafter KA95) has considered the enhancement of drag by low-level wave breaking and the trapping of the hydrostatic and non-hydrostatic GWs. Zhong et al. (2014a) implemented the KA95 scheme in the Global/Regional Assimilation and Prediction System Tropical Mesoscale Model (GRAPES_TMM), and demonstrated that the scheme improved the overall ability of GRAPES_TMM in forecasting typhoon path and intensity, as well as the cold air outbreak over South China (Zhong et al., 2014b). However, the KA95 scheme excludes the mountain blocking drag (MBD) effect, which has been considered in several other orographic drag parameterizations (Lott and Miller, 1997; hereafter LM97; Webster et al., 2003; Kim and Doyle, 2005; Wang et al., 2008). In addition to the GWD induced by SSO, the MBD induced by flows over/around complex orography also needs to be parameterized to reduce the mountain wave effect and to simulate realistic atmospheric flows.

Kim and Doyle (2005) extended the KA95 scheme by including the MBD effect in their drag parameterization. They adopted the bulk aerodynamic drag formulation, which physically resembles the parameterizations of LM97 and Scinocca and McFarlane (2000). As pointed out by LM97, the inclusion of the MBD effect improves simulation of the low-level flow deflection and resembles the effect of the enhanced orography. A drawback of the enhanced orography is that

stagnant flow effects are treated as invariant, whereas they are actually time dependent. Furthermore, envelope orography may artificially increase the modeled precipitation (Lott and Miller, 1997). This problem is averted by GRAPES_TMM, which has replaced the envelope orography with a more realistic “mean” grid-scale orography. In the present study, we modified the KA95 scheme by including the MBD in a regional model developed on the basis of GRAPES_TMM. We account for the orographic angle, anisotropy, and slope in a three-dimensional (3D) framework.

Section 2 introduces the model we used and the modified KA scheme, and summarizes the experimental design. Section 3 experimentally evaluates the impact of the modified scheme on precipitation and wind forecasts over South China in July 2013. The performance of the modified scheme is compared with that of the original KA95 scheme. A summary and discussion are presented in Section 4.

2. Model description and experimental design

2.1 GRAPES_TMM and RMSC

Based on the GRAPES_TMM (Chen et al., 2008), a regional model for South China (RMSC) was developed. The RMSC adopts a semi-implicit Lagrangian temporal difference scheme on the Arakawa-C grid with a Charney-Philip vertical layer-skipping setup. It also employs a modified hydrostatic deduction technique, a relaxed correction method in the boundary zone, and effective orography construction. The RMSC, first implemented in 2009, focuses on forecasting the weather systems over South China. It produces operational forecasts of isobaric atmospheric fields twice a day (Chen et al., 2010). Since its deployment, the RMSC has provided important reference for weather forecasters and researchers. Realtime RMSC forecasts and verification results are available at: <http://www.grapes-trams.org.cn>.

2.2 The orographic drag parameterization

In this study, the term orographic drag parameterization is abbreviated as OP. To improve the KA95 GWD scheme in the RSMC, we combined the MBD

parameterization with bluff-body dynamics (Miller, 2004) and incorporated this design into the KA95 scheme. The mesoscale flow dynamics are described by the following two conceptual schemes, whose relative importance depends on the non-dimensional mountain height. If the maximum height of a mountain range is H , its non-dimensional height (also called the inverse Froude number) is written as

$$H_n = \frac{NH}{|U|}, \quad (1)$$

where U is the horizontal wind speed and N is the Brunt–Vaisala frequency. If H_n is small, the atmospheric flow passes over the mountain and triggers orographic GWs. The corresponding stress at the reference level (the level of the generated GWD) is given by (Kim and Arakawa, 1995)

$$\tau_0 = -E \frac{m'}{\Delta x} \frac{\rho_0 U_0^3}{N_0} G', \quad (2)$$

where ρ is the atmospheric density, and Δx is the horizontal scale of the model grid. The subscript 0 denotes the reference level, i.e., the level at which GWs are generated. E is the enhancement factor of the drag force at the reference level that is used to enhance the reception of the drag force caused by lower-level wave breaking or suppression effects, which represents the number of mountains within a grid specified by m' , and G' is a progressive function for judging whether the atmospheric flow is free or blocked.

At large H_n , the vertical motion of the atmospheric flow is blocked and part of it flows around the mountain, generating the MBD. The height of the blockage (block level) is estimated by the following equation:

$$Z_{\text{blk}} = \max \left[0, h \left(1 - \frac{1}{H_n} \right) \right].$$

Unlike the GWD parameterization process, blocking drag in the MBD parameterization occurs mainly within the block level (Z_{blk}); hence, the drag force is integrated from $z = 0$ to Z_{blk} . The corresponding blocking drag is

$$\tau_{\text{blk}}(z) = -\rho_0 C_d l(z) \frac{U|U|}{2}, \quad (3)$$

$$l(z) = \frac{L^2}{2} \left(\frac{Z_{\text{blk}} - z}{z + \mu} \right)^{\frac{1}{2}} \max \left(\frac{\cos \psi}{a}, \frac{\sin \psi}{b} \right), \quad (4)$$

where $l(z)$ is the effective orographic height related to the wind direction and blocked height (Alpert, 2004), μ is an altitude above the mountain, ψ denotes the angle between the directions of the low-level wind and the principal axis of the topography, and $a \approx \mu/\sigma$ and $b \approx \frac{a}{\gamma}$ in Eq. (4) relate to SSO parameters; namely, the anisotropy σ and mean slope γ . To ensure the stability of MBD parameterization, the wind speed U in Eq. (3) is determined by a semi-implicit method that updates U at step $t+dt$ and $|U|$ at step t . The 3D GWD is parameterized by adding Eqs. (2) and (3) in the physics equations of the GRAPES model, given by

$$\frac{\partial \bar{u}}{\partial t} = -\frac{1}{\rho} \frac{\partial \bar{\tau}}{\partial z'}. \quad (5)$$

2.3 Experimental setup

The fundamental effects of MBD are investigated in two sensitivity experiments: one accounting for the 3D GWD parameterization effect (i.e., the MBD experiment considering both GWD and MBD) and the other neglecting this effect (i.e., the GWDO experiment with the original KA95 scheme considering only the GWD induced by SSO). In addition, a control (CTL) experiment without considering any orographic drag effect was also conducted. All the three experiments employed the same boundary layer, land surface, and convective parameterization schemes, and identical standard initialization (SI); namely, the Yonsei University (YSU) boundary layer scheme, the simplified Arakawa-Schubert (SAS) cumulus parameterization scheme, the SLAB land surface scheme, the SWRAD short-wave radiation scheme, and the Rapid Radiative Transfer Model (RRTM) long-wave radiation scheme. The simulation domain comprises 195×153 grid points with a horizontal resolution of 18 km, as shown in Fig. 1. There are 55 layers in the vertical direction, and both the initial and lateral boundary fields are obtained from the $0.5^\circ \times 0.5^\circ$ forecast fields of the NCEP Global Forecast System (GFS) with the lateral boundary fields updated every 6 h.

We conducted a one-month simulation for the three experiments: GWDO, CTL, and MBD. The MBD uses the modified OP scheme based on the KA95

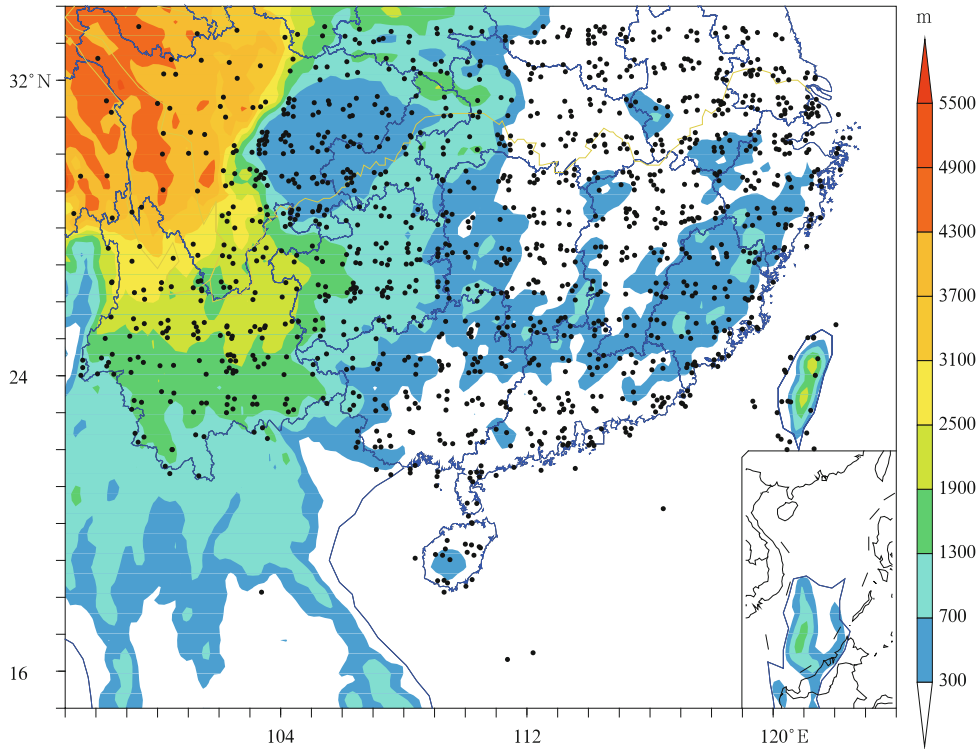


Fig. 1. Domain of the RMSC. Color shadings denote orography, and the black dots indicate locations of the 1298 automatic stations used in the RMSC verification system.

scheme. The experiment period is from 1200 UTC 19 June to 1200 UTC 21 July 2013. The verification is performed with a nationwide uniform standard verification program provided by the Center for Numerical Prediction Research, Chinese Academy of Meteorological Sciences. This system has been localized, and its validity has been confirmed in a previous operation test. We verified the 850-hPa wind, the temperature at 2 m above ground level (T_{2m}), and the 24- and 48-h forecast accumulative precipitation. The surface variables (T_{2m} and precipitation) are compared with data from 1298 automatic stations in the study domain (Fig. 1), and the isobaric variables (850-hPa winds) are examined against the GFS analysis data over 11.20° – 33.76° N, 97.40° – 128.84° E (the statistical details will be given in Section 3.4).

Especially in summer, the RMSC forecasts of low-level strong southwest winds are widely variable. Therefore, we selected a 48-h simulation of the weather patterns from 30 June to 1 July 2013, when sustained rainstorms with strong low-level southwest winds oc-

curred in the Sichuan basin. We investigated the influence of MBD on the forecasting of the low-level wind field and precipitation by the RMSC, through the GWDO experiment in parallel with an MBD experiment. As shown in Fig. 1, the RMSC domain embraces South and West China, characterized by complicated orography of plateaus and basins.

3. Results

3.1 Applicability of the MBD parameterization

As discussed in Section 2, the blocking drag is integrated from the surface up to the blocking level Z_{blk} . Palmer and Mansfield (1986) posed an upper limit on the standard deviation of the orography for the blocking level. To represent the blocking situation, Kim and Doyle (2005) expanded the definition of the Froude number to include the 3D flow over mountains. They computed the horizontal aspect ratio of the mountains, and calibrated by comparing the para-

meterized vertical distribution of the momentum flux with that obtained from explicit mesoscale simulations. In the present paper, the one-month simulation results are compared with the observation data. A critical effective height exists such that

$$H_c = \frac{KE}{PE}, \quad (6)$$

$$PE = \int_{H_c}^{h_c} N^2(h_c - z)dz, \quad (7)$$

$$KE = \frac{1}{2}u^2, \quad (8)$$

where KE and PE denote the kinetic and potential energy, respectively. According to the dividing streamline theory (Snyder et al., 1985), when $KE > PE$, the atmospheric flow passes over the mountain and triggers orographic GWs. If $KE < PE$, the flow lacks sufficient energy to rise above the mountain and is in-

stead forced around it, generating MBD. Hence, the block layer forms when PE exceeds KE, and MBD is calculated between the surface and the block layer.

As the terrain height over the Sichuan basin is approximately 300 m (see Fig. 1), we analyzed the KE and PE at 417 m. Figure 2 shows the distributions of KE and PE at 417 m after 10 h of model integration, as well as the related blocking area calculated in the MBD parameterization. PE exceeds KE everywhere except in the central Sichuan basin, a characteristically low-lying region. High PE flows are concentrated around steep mountains (see topographical details in Fig. 1), whereas their high KE counterparts dominate the northwest of Sichuan and may cause GWD as they pass over mountainous regions. In other words, it is necessary to apply the MBD parameterization over the complicated geography of the Sichuan basin. The

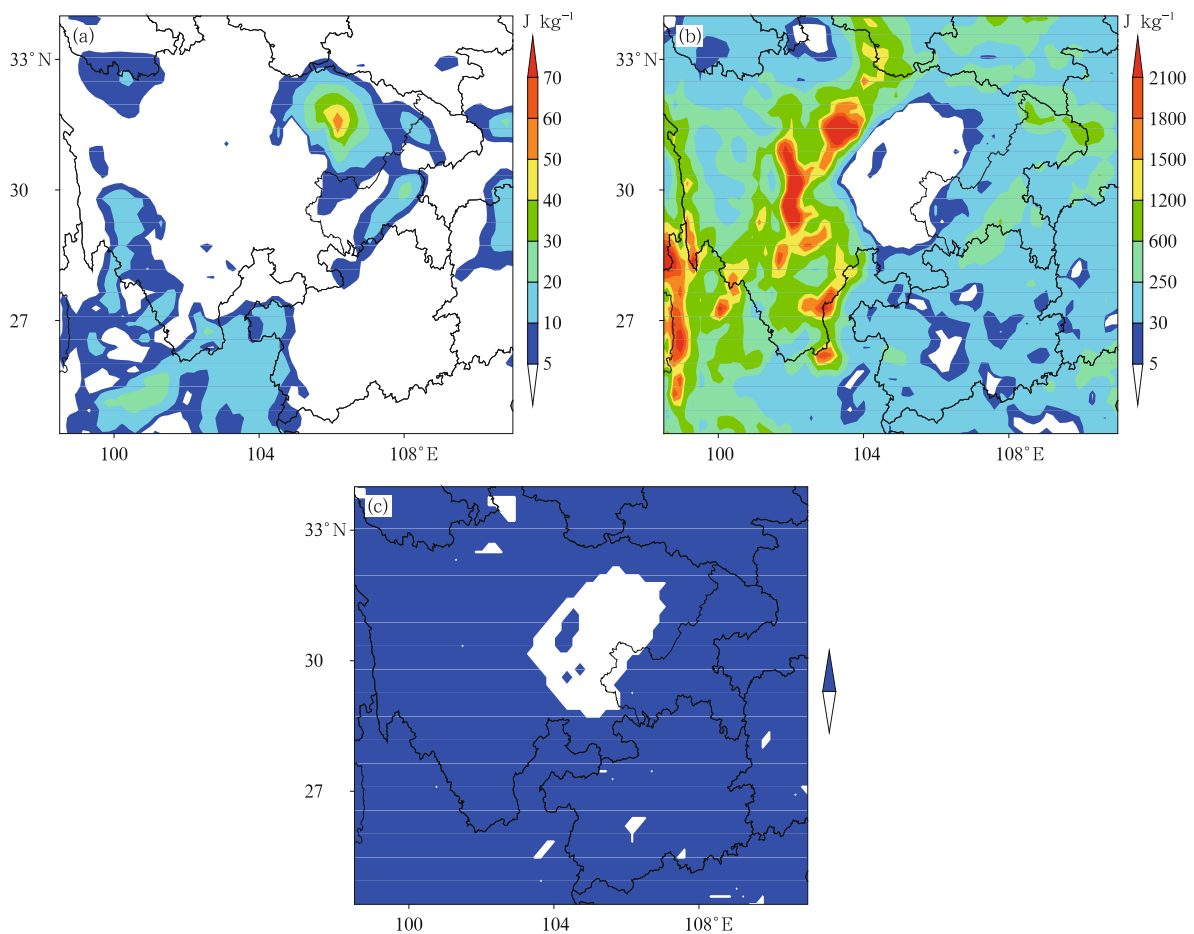


Fig. 2. (a) KE, (b) PE, and (c) the corresponding blocking drag region (blue shading denotes the MBD parameterization applicable area), at 417 m above the surface after 10-h model integration.

blocking drag at different levels and its effect on the wind field are discussed next.

3.2 The MBD effect

Figure 3 shows the MBD values at 417 and 4109 m. The large value area covers the eastern low-lying region and the western steep mountains around the Sichuan basin. The drag magnitude is much higher in the eastern than in the western region; consequently, the wind disturbance (accelerated wind speed determined by MBD) is stronger in the east of Sichuan basin. In other words, a large amount of surface stress exists in the eastern region, triggering appreciable wind disturbance in the low troposphere. Figure 3 reveals a striking drag stress east of the Sichuan basin, where the wind toward south meets the windward mountain. This drag may trigger GWs and transport the kinetic energy, thereby redistributing the wind field and altering the convergence and moisture distribution. These conditions are ideal for precipitation. According to observations at the automatic weather stations over East Sichuan, several heavy rainfall events did occur in Guangyuan Municipality of Sichuan on 1, 18, and 19 July 2013. Hence, we study the effects of MBD parameterization on the wind field and precipitation over the above area.

Figure 4 presents the vertical velocity differences

between the MBD and GWDO experiments at 850 and 500 hPa. The MBD parameterization introduces significant changes to the middle and lower troposphere. Specifically, it generates disturbances in the wind field, especially over the east of Sichuan. The ascending motion is accelerated in the affected region, and the cyclonic circulation is also strengthened. We conclude that the wind circulation over complex topography is

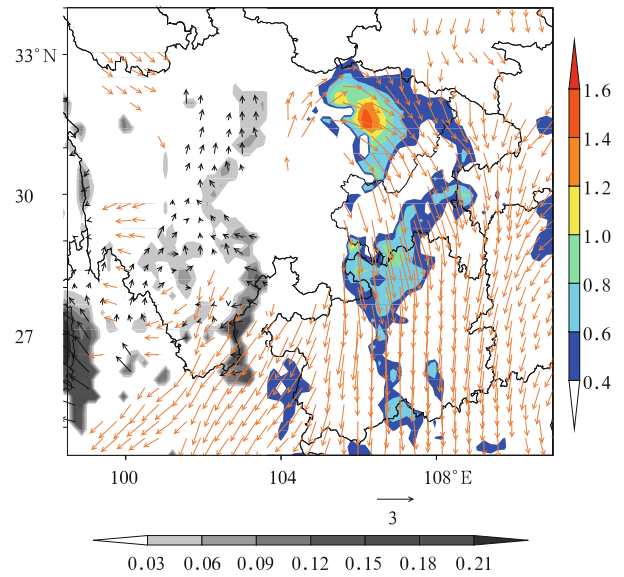


Fig. 3. The stress of MBD (10^{-2} N m^{-2}) and wind turbulence (10^{-5} s^{-1}) at 417 m (vertical rainbow scale) and 4109 m (horizontal gray scale) after 10-h model integration.

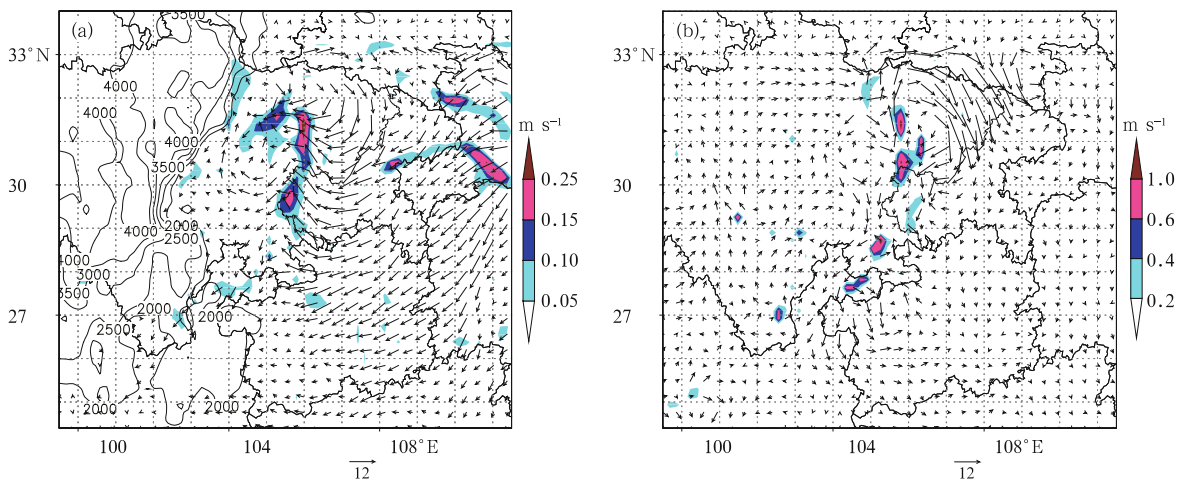


Fig. 4. Vertical wind speed (shaded) and horizontal wind difference (arrows) between the MBD and GWDO experiments (MBD–GWDO) at (a) 850 and (b) 500 hPa, valid at 0200 UTC 1 July 2013 (14-h forecast time). The contours in (a) represent terrain height.

especially sensitive to the MBD parameterization in numerical weather prediction models. The MBD parameterization also affects other simulated fields, such as the convergence (divergence), vorticity, and water vapor transport in the atmosphere. This indicates that good simulations of an atmospheric model depend to a certain degree on successful parameterization of the MBD effect.

3.3 Short-range forecast

As discussed in Section 2, when the GWD induced by SSO is included in the model physics, the resulting GWD significantly affects the kinetic energy dissipation. This dissipation is essential to the short-range forecasting of wind fields, accumulative precipitation, and other meteorological factors. In this subsection, we analyze the effect of MBD on the lower troposphere wind and accumulative precipitation forecasting. Figure 5 compares the moisture convergence and low-level jets simulated in the MBD and GWDO experiments. The MBD parameterization significantly alters the maximum wind field at 850 hPa. The area of the winds greater than 12 m s^{-1} is closer to northern and northeastern Sichuan basin in the MBD experiment than in the GWDO experiment, and the bulk wind direction changes from southwesterly in the GWDO ex-

periment to southerly in the MBD experiment. Therefore, the MBD parameterization strengthens moisture convergence in the heavy rainfall region east of Sichuan and enhances the ascending motion in that region. These modifications significantly impact the precipitation forecasts.

Figure 6 shows the 24-h precipitation forecast in MBD and GWDO experiments. The center of heavy rainfall and the position of the 24-h rain belt simulated in the MBD experiment are in better agreement with the observations at 1200 UTC 30 June 2013. More striking improvements on the precipitation forecast are observed at 0000 UTC 1 July 2013. The magnitude and area of the precipitation are significantly improved by the MBD parameterization, especially in forecasting of the 24-h rainfall exceeding 50 mm. By contrast, the GWDO experiment yields much weak precipitation.

The MBD affects the wind forecasts at almost all forecast times. The analysis field and 24-h simulations of 850-hPa wind in MBD and GWDO experiments at 1200 UTC 1 July 2013 are plotted in Fig. 7. It is found that the excessively strong southerly wind over southeast Sichuan is substantially alleviated by the MBD parameterization. In the GWDO experiment, the strong southerly wind in that region exceeds 16

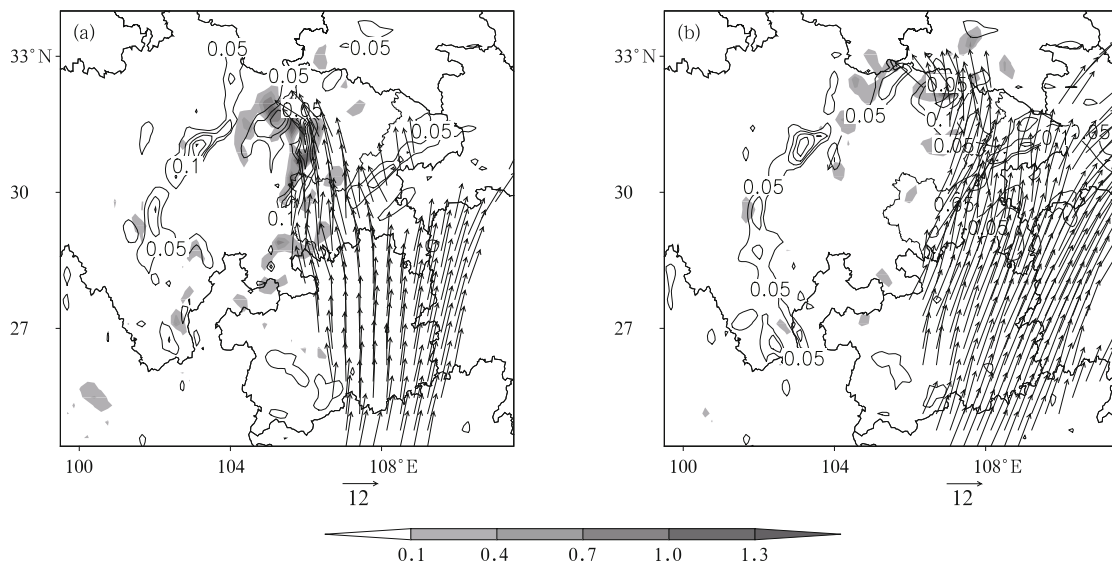


Fig. 5. Simulated moisture convergence (shaded; $10^{-7} \text{ g m kg}^{-1} \text{ s}^{-1}$), vertical velocity (contours), and low-level wind (vectors; $> 12 \text{ m s}^{-1}$) at 850 hPa in (a) MBD and (b) GWDO experiment, at 0200 UTC 1 July 2013.

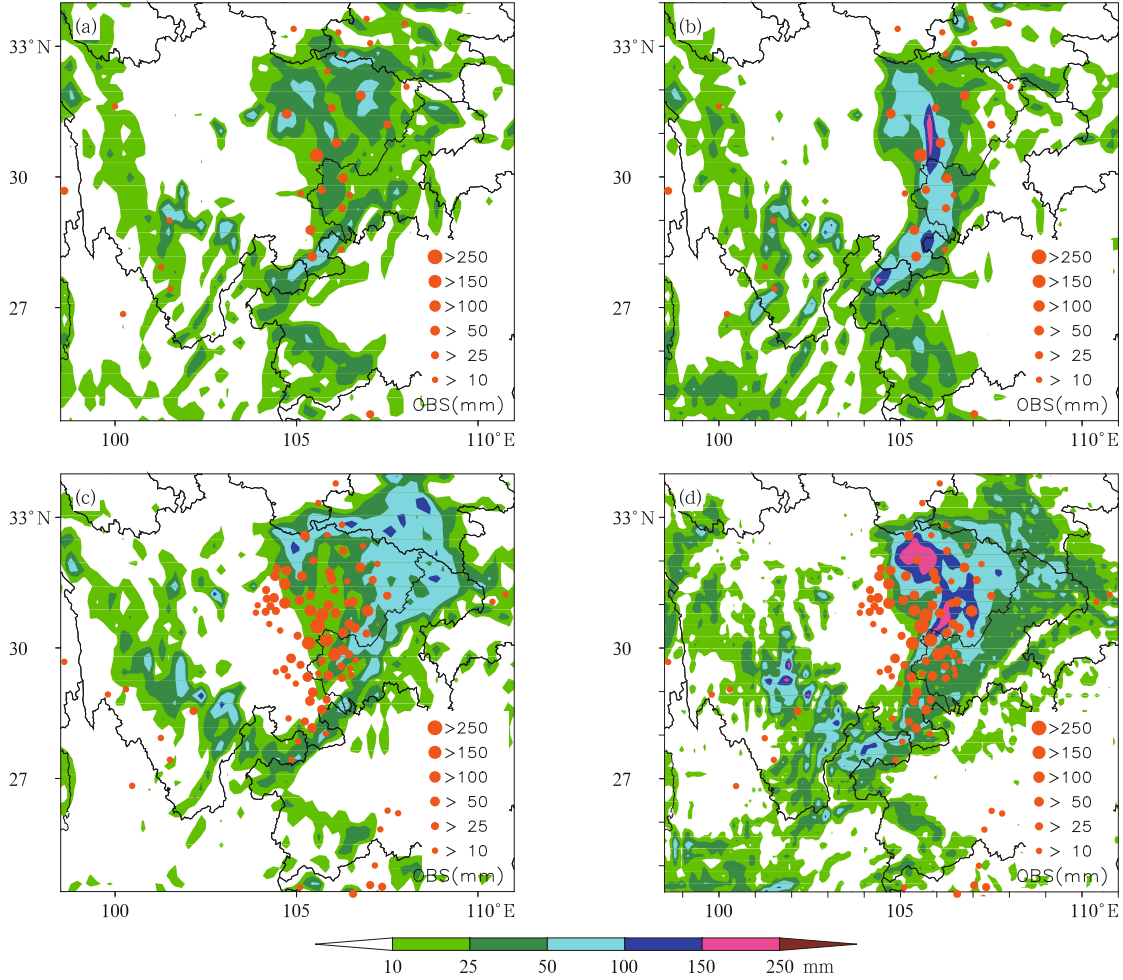


Fig. 6. The 24-h accumulative precipitation from (a, c) GWDO and (b, d) MBD experiments at (a, b) 1200 UTC 30 June and (c, d) 0000 UTC 1 July 2013. The red dots represent observed values.

m s^{-1} (Fig. 7c), but reduces to approximately 12 m s^{-1} in the MBD experiment (Fig. 7b), showing an improvement on the wind forecast in the lower troposphere, compared with the GFS analysis (Fig. 7a). In the simulated 700-hPa vorticity field (figure omitted), the intensity of the low-vorticity center is closer to that of the GFS analysis in MBD than in CTL. Without the blocking drag parameterization, the low-vorticity center is too strong over Sichuan Province.

3.4 Monthly verification

To verify the effects of the modified OP scheme, we conducted a month-long verification starting from 1200 UTC 19 June 2013 using the verification program provided by the Center for Numerical Prediction Research, Chinese Academy of Meteorological Sciences.

The verified variables include the wind field at 850 hPa and $T_{2\text{m}}$. The root-mean-square error (RMSE) between the forecast and observation is calculated, and the 24-h precipitation (24P) threat scores (TSs) at 5 levels, i.e., LR ($24\text{P} \leq 9.9 \text{ mm}$), MR ($10 \text{ mm} \leq 24\text{P} \leq 24.9 \text{ mm}$), SR ($25 \text{ mm} \leq 24\text{P} \leq 49.9 \text{ mm}$), HR ($50 \text{ mm} \leq 24\text{P} \leq 99.9 \text{ mm}$), and SHR ($100 \text{ mm} \leq 24\text{P} \leq 249.9 \text{ mm}$), are also computed. Here, the larger the TS values, the better the model forecast of precipitation. The RMSE is calculated as follows:

$$\text{RMSE} = \left[\frac{1}{N} \sum (F - A_v)^2 \right]^{\frac{1}{2}},$$

where F and A_v are the forecasted and analysis values, respectively, and N is the number of grid points in the verification region. In verifying the 850-hPa wind

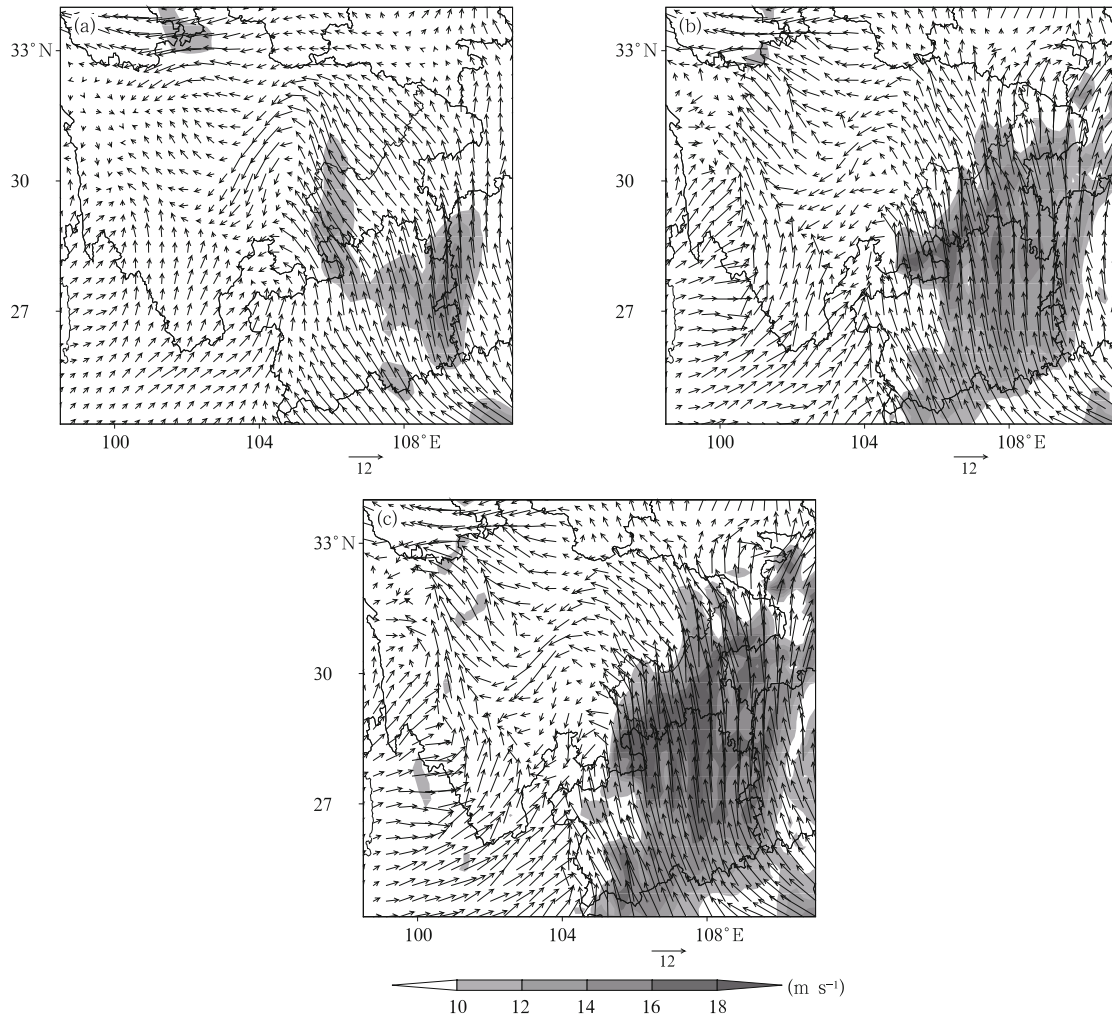


Fig. 7. Total wind speed (shaded) and wind vectors at 850 hPa at 0000 UTC 1 July 2013 from the (a) NCEP GFS analysis field, (b) MBD, and (c) GWDO experiment.

field, the NCEP analysis is used as the analysis value, whereas in verifying the temperature at 2 m above ground level, the ground-level SYNOP data collected by the South China Regional Meteorological Center at 1298 observation stations are used as the observed

data. The stations are distributed as shown in Fig. 1.

Table 1 presents the verification scores of the 24- and 48-h forecasts from the MBD, GWDO, and CTL experiments. Shown are RMSEs and TSs over South China. The results demonstrate the overall improve-

Table 1. Skill scores of RMSE and TS for the meteorological variables at 24- and 48-h forecast time in MBD, GWDO, and CTL experiments over 11.2°–33.76°N, 97.4°–128.84°E for the extremely heavy rainfall process over the Sichuan basin from 1200 UTC 19 June to 1200 UTC 21 July 2013

		24-h forecast			48-h forecast		
		MBD	GWDO	CTL	MBD	GWDO	CTL
RMSE	850-hPa wind	3.93	4.36	4.79	4.94	5.17	5.61
	T_{2m}	2.49	2.48	2.48	3.05	3.07	3.09
TS	LR	0.64	0.63	0.63	0.62	0.62	0.62
	MR	0.31	0.31	0.30	0.27	0.26	0.26
	SR	0.20	0.20	0.20	0.14	0.14	0.14
	HR	0.11	0.10	0.09	0.07	0.07	0.07
	SHR	0.03	0.02	0.02	0.02	0.01	0.01

ments of the modified OP scheme. RMSEs of the 24- and 48-h forecasts of the 850-hPa wind and those of T_{2m} are reduced by the modified OP. In particular, the RMSE of the 24-h 850-hPa wind forecast reduces from 4.36 m s^{-1} in the GWDO experiment to 3.93 m s^{-1} in the MBD experiment, while that of the 48-h forecast decreases from 5.17 to 4.94 m s^{-1} . In other words, the modified OP reduces the RMSEs in the 24- and 48-h 850-hPa wind forecasts by 0.43 and 0.23 m s^{-1} , respectively. Clearly, the RMSEs of the 24- and 48-h forecasts of the 850-hPa wind are much larger in the CTL experiment than in MBD and GWDO experiments, indicating that parameterizing the GWD induced by SSO alleviates biases in low-level wind forecasting. The RMSEs of T_{2m} (the TS values of precipitation) are slightly smaller (larger) in the MBD experiment than in GWDO and CTL experiments. The MBD parameterization has mainly improved the 24- and 48-h forecasting of LR, MR, HR, and SHR.

4. Summary and discussion

To improve the forecasting of wind circulation and precipitation over South China, we implemented a modified OP scheme in the RMSC developed from the GRAPES_TMM. The simulation using the modified OP scheme that accounts for the MBD effect successfully captured the main features of the precipitation, including its distribution and intensity, and also improved forecast of the lower tropospheric wind circulation, demonstrating an overall improvement in model performance.

This study did not investigate the effect of MBD parameterization beyond 48 h. It did not compare the gravity wave breaking criteria with observation data either. Rather, we compared explicitly simulated wind fields and 24-h precipitation forecasts generated by the OP scheme and by the modified OP. On the other hand, Kim and Doyle (2005) evaluated the orographic drag parameterization by calculating the surface pressure drag, which is essential to verify the GWD parameterization induced by SSO in the physical model. Kim and Hong (2009) suggested that GWD is sensitive to the boundary layer scheme and shortwave radiation scheme (Shin et al., 2010). The

sensitivity of MBD to the land surface scheme is also worthy of investigation. Furthermore, the boundary fluxes could be verified by calculating the vertical Reynolds stress profiles (Laprise and Peltier, 1989), as well as the self-acceleration in the parameterization of GWD (Scinocca and Sutherland, 2010), wave resonance (Grubišić and Stiperski, 2009; Teixeira et al., 2012) and wave breaking in directionally sheared flows (Teixeira, 2014), which were not considered in the present paper.

In summary, parameterization of the MBD effect in different orographical settings is necessary for better simulating the atmospheric processes, especially over large-scale orography such as the southwestern regions of China. The modified OP scheme might also influence the cold air outbreak into southern China, particularly in winter and spring. This influence has important implications for weather forecast and related application, and will be investigated in future work.

Acknowledgments. The authors are thankful to Dr. Meng Weiguang for his enthusiastic and rigorous comments to this article. The comments from the anonymous reviewers are also appreciated.

REFERENCES

- Alpert, J. C., 2004: Sub-grid scale mountain blocking at NCEP. Proceedings of the 16th conference on NWP, Seattle, Washington, Amer. Meteor. Soc., 2–4.
- Bauer, M. H., G. J. Mayr, I. Vergeiner, et al., 2000: Strongly nonlinear flow over and around a three-dimensional mountain as a function of the horizontal aspect ratio. *J. Atmos. Sci.*, **57**, 3971–3991.
- Boer, G. J., N. A. Mcfarlane, R. Laprise, et al., 1984: The Canadian Climate Centre spectral atmospheric general circulation model. *Atmos. Ocean*, **22**, 397–429.
- Broccoli, A. J., and S. Manabe, 1992: The effects of orography on midlatitude Northern Hemisphere dry climates. *J. Climate*, **5**, 1181–1201.
- Chen Dehui, Xue Jishan, Yang Xuesheng, et al., 2008: New generation of a multi-scale NWP system (GRAPES): General scientific design. *Chin. Sci. Bull.*, **53**, 3433–3445.
- Chen Zitong, Huang Yanyan, Wan Qilin, et al., 2010: Rapid updating cycle assimilation forecasting sys-

- tem and its experimental analysis in flood season. *J. Trop. Meteor.*, **26**, 49–54. (in Chinese)
- Grubišić, V., and I. Stiperski, 2009: Lee-wave resonances over double bell-shaped obstacles. *J. Atmos. Sci.*, **66**, 1205–1228.
- Helfand, H. M., J. C. Jusem, J. Pfaendtner, et al., 1987: The effect of a gravity wave drag parameterization scheme on GLA fourth order GCM forecast. *J. Meteor. Soc. Japan*, Special volume for the WMO/IUGG NWP Symposium, Tokyo, Japan, 729–742.
- Helfand, H. M., and J. C. Labraga, 1988: Design of a nonsingular level 2.5 second-order closure model for prediction of the atmospheric turbulence. *J. Atmos. Sci.*, **45**, 113–132.
- Hong, S. Y., C. Jung, E. C. Chang, et al., 2008: Lower-tropospheric enhancement of gravity wave drag in a global spectral atmospheric forecast model. *Wea. Forecasting*, **23**, 523–531.
- Kim, Y.-J., and A. Arakawa, 1995: Improvement of orographic gravity-wave parameterization using a mesoscale gravity-wave model. *J. Atmos. Sci.*, **52**, 1875–1902.
- Kim, Y.-J., J. D. Farrara, and C. R. Mechoso, 1998: Sensitivity of AGCM simulations to modifications in the ozone distribution and refinements in selected physical parameterizations. *J. Meteor. Soc. Japan*, **76**, 695–709.
- Kim, Y.-J., and J. D. Doyle, 2005: Extension of an orographic-drag parametrization scheme to incorporate orographic anisotropy and flow blocking. *Quart. J. Roy. Meteor. Soc.*, **131**, 1893–1921.
- Kim, Y.-J., and S. Y. Hong, 2009: Interaction between the orography-induced gravity wave drag and boundary layer processes in a global atmospheric model. *J. Geophys. Res.*, **36**, L12809, doi: 10.1029/2008GL037146.
- Laprise, R., and W. R. Peltier, 1989: The structure and energetics of transient eddies in a numerical simulation of breaking mountain waves. *J. Atmos. Sci.*, **46**, 565–585.
- Lilly, D. K., 1972: Wave momentum flux—A GRAP problem. *Bull. Amer. Meteor. Soc.*, **53**, 17–23.
- Lindzen, R. S., 1981: Turbulence and stress owing to gravity wave and tidal breakdown. *J. Geophys. Res.*, **86**, 9707–9714.
- Lott, F., and M. J. Miller, 1997: A new subgrid-scale orographic parameterization: Its formulation and testing. *Quart. J. Roy. Meteor. Soc.*, **123**, 101–127.
- Matsuno, T., 1982: A quasi one-dimensional model of the middle atmosphere circulation interacting with internal gravity waves. *J. Meteor. Soc. Japan*, **60**, 215–226.
- McLandress, C., T. G. Shepherd, S. Polavarapu, et al., 2012: Is missing orographic gravity wave drag near 60°S the cause of the stratospheric zonal wind biases in chemistry–climate models? *J. Atmos. Sci.*, **69**, 802–818.
- McLandress, C., J. F. Scinocca, T. G. Shepherd, et al., 2013: Dynamical control of the mesosphere by orographic and nonorographic gravity wave drag during the extended northern winters of 2006 and 2009. *J. Atmos. Sci.*, **70**, 2152–2169.
- Miller, M. J., 2004: Subgrid-scale orographic drag. Meteorological Training Course Lecture Series for ECMWF, 1–9.
- Miller, M. J., T. N. Palmer, and R. Swinbank, 1989: Parameterization and influence of subgrid-scale orography in general circulation and numerical weather prediction models. *Meteor. Atmos. Phys.*, **40**, 84–109.
- Palmer, T. N., and D. A. Mansfield, 1986: A study of wintertime circulation anomalies during past El Niño events, using a high resolution general circulation model. I: Influence of model climatology. *Quart. J. Roy. Meteor. Soc.*, **112**, 613–638.
- Palmer, T. N., G. J. Shutts, and R. Swinbank, 1986: Alleviation of a systematic westerly bias in general circulation and numerical weather prediction models through an orographic gravity wave drag parameterization. *Quart. J. Roy. Meteor. Soc.*, **112**, 1001–1039.
- Qian, Y. F., 2000: Effects of envelope orography and gravity wave drag on performance of climate modeling. *J. Appl. Meteor. Sci.*, **11**, 13–20. (in Chinese)
- Scinocca, J. F., and N. A. McFarlane, 2000: The parameterization of drag induced by stratified flow over anisotropic topography. *Quart. J. Roy. Meteor. Soc.*, **126**, 2353–2393.
- Scinocca, J. F., and B. R. Sutherland, 2010: Self-acceleration in the parameterization of orographic gravity wave drag. *J. Atmos. Sci.*, **67**, 2537–2546.
- Shin, H. H., S. Y. Hong, J. Dudhia, et al., 2010: Orography-induced gravity wave drag parameterization in the global WRF: Implementation and sensitivity to shortwave radiation schemes. *Adv. Meteor.*, doi: 10.1155/2010/959014.

- Snyder, W. H., R. S. Thompson, R. E. Eskridge, et al., 1985: The structure of strongly stratified flow over hills, dividing-streamline concept. *J. Fluid Mech.*, **152**, 249–288.
- Teixeira, M. A. C., 2014: The physics of orographic gravity wave drag. *Front Phys.*, **2**, 43, doi: 10.3389/fphy.2014.00043.
- Teixeira, M. A. C., J. L. Argáinband, and P. M. A. Miranda, 2012: The importance of friction in mountain wave drag amplification by Scorer parameter resonance. *Quart. J. Roy. Meteor. Soc.*, **138**, 1325–1337.
- Wang Yuan, Cai Ninghao, and Tang Jinyun, 2008: A Two-wave scheme for orographic gravity wave drag parameterization. *J. Meteor. Res.*, **22**, 152–161.
- Webster, S., A. R. Brown, D. R. Cameron, et al., 2003: Improvements to the representation of orography in the Met Office Unified Model. *Quart. J. Roy. Meteor. Soc.*, **129**, 1989–2010.
- Zhong Shuixin, Chen Zitong, Dai Guangfeng, et al., 2014a: Impacts of orographic gravity wave drag parameterization on typhoon intensity and path. *Chinese J. Atmos. Sci.*, **38**, 273–284. (in Chinese)
- Zhong Shuixin, Chen Zitong, Huang Yanyan, et al., 2014b: Applying orography-induced gravity wave drag parameterization to GRAPES model. *J. Trop. Meteor.*, **30**, 413–422. (in Chinese)